Primljen / Received: 16.6.2022.
Ispravljen / Corrected: 25.12.2023.
Prihvaćen / Accepted: 30.1.2024.
Dostupno online / Available online: 10.4.2024.

Temperature–water–load coupling study on stress characteristics of BFRP–CRCP pavement

Authors:

Xueling Chen, MCE
Northeast Forestry University, China
Faculty of Civil Engineering
cxlteacher@126.com

Prof. **Lifeng Wang**, PhD. CE
Northeast Forestry University, China
Faculty of Civil Engineering
DCXL198302@163.com
Corresponding author

Research Paper

Xueling Chen, Lifeng Wang

Temperature–water–load coupling study on stress characteristics of BFRP–CRCP pavement

The stress characteristics of continuously reinforced concrete pavements with basalt fibre-reinforced bars (BFRP–CRCP) were investigated using the temperature–water–load coupling theory, based on the characteristics of frozen soil in Northeast China, combined with existing research experience, and taking the foundation thaw settlement effect in Northeast China as a starting point. The COMSOL finite element software was used to create a finite element model of the BFRP–CRCP subgrade and pavement China. Several common affecting elements, such as pavement thickness, reinforcement ratio, and concrete modulus, were examined, and appropriate recommendations for BFRP–CRCP pavement material selection were made. Further, the stress characteristics of the BFRP–CRCP pavement structure combination were investigated utilising three common structural forms of pavement in the region and focusing on distinct contributing elements. It serves as a model for BFRP–CRCP pavement construction that considers settlement deformation.

Key words:
frozen soil, BFRP–CRCP, settlement deformation, pavement

Prethodno priopćenje

Xueling Chen, Lifeng Wang

Utjecaj temperature, vode i opterećenja na karakteristike naprezanja BFRP-CRCP kolnika

Karakteristike naprezanja kontinuirano armiranobetonskih kolnika sa šipkama ojačanima bazaltnim vlaknima (BFRP–CRCP) ispitane su primjenom teorije povezanosti temperature, vode i opterećenja, temeljene na svojstvima smrznutog tla u sjeveroistočnoj Kini, u kombinaciji s postojećim istraživačkim iskustvom. Za polaznu je točku uzet utjecaj slijeganja temeljnog tla uslijed odmrzavanja u sjeveroistočnoj Kini. Računalni program COMSOL primijenjen je za izradu modela konačnih elemenata BFRP-CRCP temeljnog tla i kolničke konstrukcije u Kini. Ispitani su osnovni utjecajni elementi poput debljine kolnika, koeficijenta armiranja i modula elastičnosti betona te su dane odgovarajuće preporuke za odabir materijala za BFRP-CRCP kolnik Kini. Nadalje, karakteristike naprezanja kombinirane BFRP-CRCP kolničke konstrukcije ispitane su primjenom triju najčešće korištenih kolničkih konstrukcija u regiji uz fokus na različite elemente koji im doprinose. Navedeno služi kao model za BFRP-CRCP kolničku konstrukciju, pri čemu se uzimaju u obzir deformacije uslijed slijeganja.

Ključne riječi:
smrznuto tlo, BFRP-CRCP, deformacija uslijed slijeganja, kolnik

1. Introduction

Frozen soil is extensively dispersed throughout China, with seasonally frozen soil and permafrost accounting for more than 70 % of the total geographical area. Permafrost spans around 2.15 million square kilometres, accounting for one-fifth of China's geographical area and ranking third in the world, primarily in the northeast and the Qinghai–Tibet Plateau. Northeast China has almost 3,839,000 square kilometres of permafrost, which is classified as 'low altitude, high latitude' permafrost. In addition to permafrost, most of the northeast is seasonally frozen. Northeast China is rich in natural resources; however, its economic growth has been delayed by its cold environment and inadequate infrastructure. In recent years, the state has boosted infrastructure investments in the northeastern region, including the construction of multiple roadways at different levels. Freeze–thaw geological catastrophes such as frost heave and thaw collapse are common in frozen soil locations because of the low temperature and considerable temperature difference between day and night. Uneven settlement of the pavement structure will develop, resulting in extra stress. Roadway deformation or damage occurs due to vehicle loads and increased stress [1, 2].

American experts originally studied continuously reinforced concrete pavements (CRCP) to tackle different types of pavement distress. The CRCP was supplied with adequate steel bars in the longitudinal and transverse directions of the pavement to avoid cracking caused by the longitudinal shrinkage of the cement concrete pavement slab. The CRCP does not instal expansion and contraction joints (except for those required for building joints and structures), resulting in a full, level surface and improved driving stability. Additionally, the total strength of the road panels has improved [3-5]. The CRCP has been explored by several researchers since the late 1980s [6-10].

2. Proposing questions

Owing to its distinct benefits, the CRCP is widely employed in China. However, if CRCP cracks emerge owing to environmental causes, the steel bars in the concrete rust, reducing the overall durability of the pavement structure. Basalt fibre reinforcement outperforms steel bars in terms of strength, corrosion resistance, lightweight, and ease of transportation; further, its temperature shrinkage coefficient is comparable to that of cement concrete. More importantly, the basalt fibre reinforcement production method is pollution-free and is a novel environmental protection material. When steel bars are replaced with basalt fibre-reinforced bars (BFRP) in a CRCP, the pavement performance improves, and its service life is prolonged [28]. Because of China's vast basalt and cement resources, BFRP–CRCP roads are critical for enriching the varieties of CRCP and expanding new technologies and methods for pavements with broad application prospects. Xingyu [11] analysed and compared the application of basalt fibre rods and steel rebars in pavement engineering and concluded that, in theory, it is entirely feasible to use continuous basalt fibre rods to replace steel rebars in pavement projects.

The benefits of BFRP–CRCP are clear, and research on BFRP–CRCP in Northeast China is still in its early stages [12-16]. Northeast China's frozen soil undergoes two physical processes: freezing and thawing, resulting in the thawing settlement of subgrade soil and cracking of cement concrete pavement slabs. The stress characteristics of BFRP–CRCP were investigated in this study using the temperature–water–load coupling theory and the foundation thaw settlement impact in Northeast China as the breaking point. The COMSOL finite element software was used to create a BFRP–CRCP finite element model and several common influencing elements, such as pavement thickness, reinforcement ratio, and concrete modulus, as well as the effect law of the stress characteristics of various BFRP–CRCP materials and structural shapes. There have been reasonable proposals for the structural form and material selection of BFRP–CRCP.

3. Coupling theory

The frozen soil subgrade deforms owing to the thawing settlement of soil inside the subgrade, and the thawing settlement phenomenon necessitates the introduction of the temperature–water–load three-field coupling theory [15-22]. To facilitate the analysis, the following basic hypotheses were established: the subgrade soil is an isotropic homogeneous soil; the soil is a small linear elastic deformation body; the soil particles, ice, and water in the soil are incompressible; and the subgrade soil has thaw settlement deformation under the action of load and expansive force caused by soil freezing. COMSOL software was used for the model in this study. The three temperature, water, and load coupling equations are as follows:

a) The continuous equation of water movement in soil can be obtained based on the mass conservation law of continuum mechanics [29]:

$$\frac{\partial \theta_u}{\partial t} = \frac{\partial}{\partial_z}\left[D\frac{\partial \theta_u}{\partial z} - K\right] - \frac{\rho_i}{\rho_w}\frac{\partial \theta_i}{\partial t} \tag{1}$$

where θ_u is the volume content of unfrozen water in the soil (%), θ is the volume content of ice in the soil (%), D and K are the diffusion coefficient (m^2 / h) and conductivity coefficient (m/h), respectively, ρ_w is the water bulk density (kg / m^3), and ρ is the ice bulk density (kg / m^3).

b) Similarly, according to the mass conservation and heat conduction laws of continuum mechanics, the basic equation of the temperature field is [29]:

$$C_{vs}\frac{\partial T}{\partial t} = \frac{\partial}{\partial_z}\left[\lambda\frac{\partial T}{\partial z}\right] + L\rho_i\frac{\partial \theta_i}{\partial t} \tag{2}$$

where T is temperature (°C), C_{vs} is the volume specific heat capacity (kJ/(m · °C)), λ is the heat conductivity (KJ / (m · h · °C)), L is the linear length of the seepage path, ρ_w is the water bulk density (kg/m³), and ρ is the ice bulk density (kg/m³).

c) The deformation of the subgrade in the frozen soil area primarily considers the compression deformation caused by thaw settlement under an external load. According to the theory of elastic mechanics, the basic equation of the stress field is [29]:

$$\rho \frac{\partial^2 U}{\partial t^2} = \nabla \sigma = F \tag{3}$$

where U is displacement, F is external load, σ is the stress, and ρ is the density of soil.

4. Numerical simulation

Some basic assumptions were made in this research: BFRP–CRCP was employed in this research, and the cracks generated by dry shrinkage and temperature shrinkage of the concrete pavement were relatively small and could be ignored. The concrete pavement slab is modelled as a continuous and complete slab, and the deformation of the basalt fibre reinforcement and concrete is coordinated without considering the slip between them. The remaining layers of the pavement are isotropic linear elastic; the concrete surface layer, base layer, and subgrade are all completely continuous; and based on the satisfactory mechanical properties of the basalt fibre rods, it is considered that these rods remain in the elastic deformation range throughout the analysis process. For the constitutive relationship of the concrete, the Ottosen full-range [25] constitutive model was selected. Model establishment: the BFRP bars and concrete were modelled independently.

4.1. Model parameter setting

The cement concrete surface layer, cement-stabilised macadam foundation, and lime–soil base comprised the BFRP–CRCP pavement construction. Table 1 lists the key structural parameters of this pavement.

According to the geological parameters of the seasonally frozen soil area in Northeast China [6], the foundation fill was made from the top to bottom of gravelly sandstone, gravelly sand, and severely weathered mudstone. Table 2 displays the distinctive characteristics of each layer of the foundation soil. The thickness of the soil foundation in this study was 20 m. Figure 1 shows the subgrade and pavement construction.

Table 1. Main parameters of the BFRP–CRCP pavement structure

Pavement structural layer	Model thickness [cm]	Elastic modulus [GPa]	Poisson's ratio	Density [kg·m³]	Thermal conductivity [W/m°C]	Linear expansion coefficient [10^{-5} °C^{-1}]
Cement concrete surface	22	30.0	0.20	2643	1.4	1.0
Cement stabilized macadam base	20	1.4	0.25	2000	1.3	0.8
Lime soil subbase	20	1.5	0.30	1870	1.0	0.6

Table 2. Values of subgrade soil characteristic parameters

Physics parameters	Dry density [kg·m^{-3}]	Initial moisture content [%]	Specific heat [J·kg^{-1}·°C^{-1}]				Thermal conductivity [W·m^{-1}·°C^{-1}]		Water diffusion coefficient [μ·m^{-1}·s^{-1}]	Temperature gradient [1/degC]	Latent heata [kJ·kg^{-1}]	Empirical coefficient
			Thawed soil skele-ton	Frozen soil skele-ton	Water	Ice	Thawed soil	Frozen soil				
Gravel gravel soil	1800	25	790	710	4182	2090	1.92	1.98	9.35	-0.20	334.56	0.61
Fine sand in pebbles	1700	30	840	730	4182	2090	1.95	2.69	46.60	-0.10	334.56	0.73
Strongly weathered rock	1500	30	840	750	4182	2090	1.47	1.82	3.44	-0.05	334.56	0.47

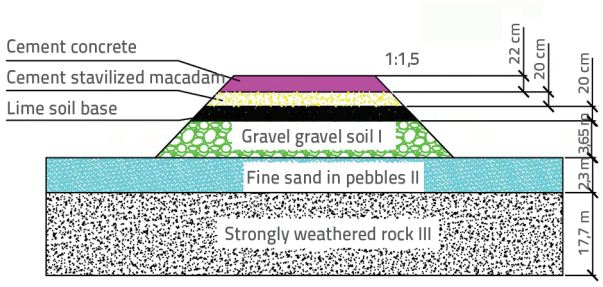

Figure 1. Roadbed and pavement cross-section

4.2. Boundary condition setting

1. Boundary conditions of temperature field

Based on observational data from permafrost regions over the years [30], without considering the temperature increase caused by global warming and in conjunction with the interfacial layer theory, the upper boundary temperature of the permafrost subgrade model was simplified into the following trigonometric expression with an annual period [31]:

$$T = T_{\alpha} + \Delta T + A \cdot \sin\left(\frac{2\pi}{360}t + \frac{\pi}{2}\right) \quad (4)$$

In the equation, T_a represents the average annual temperature of the region, and T_a was taken as -3.0 °C; ΔT is the total temperature increment considering the effect of the interfacial layer, and ΔT of the roadbed surface, roadbed slope, and natural ground surface was taken as 6.5 °C, 4.0°C and 2.5 °C, respectively; and A represents the temperature amplitude at the bottom of the interfacial layer, and A of the roadbed surface, roadbed slope, and natural ground surface was taken as 15.15 °C, 14.5 °C and 11.5 °C respectively.

Without considering the effects of sunny and shady slopes, the temperatures of the roadbed surface, roadbed slope, and natural ground surface can be expressed separately as

$$T_1 = 3{,}5 + 15{,}15 + A \cdot \sin\left(\frac{2\pi}{360}t + \frac{\pi}{2}\right) \quad (5)$$

$$T_2 = 1{,}0 + 14{,}55 + A \cdot \sin\left(\frac{2\pi}{360}t + \frac{\pi}{2}\right) \quad (6)$$

$$T_3 = -0{,}5 + 11{,}5 + A \cdot \sin\left(\frac{2\pi}{360}t + \frac{\pi}{2}\right) \quad (7)$$

According to observational data, within a certain depth below the natural surface in permafrost regions, the variation in the ground temperature is very small. In the model, it was approximated to -1.0 °C based on actual observational data and set as the boundary condition for the bottom of the model. The sides of the roadbed were thermally insulated boundaries.

2. Mechanical boundary conditions

In this study, only the subgrade settlement was included owing to the temperature change; hence, the upper surface of the model was a free boundary. The model's left and right sides can move vertically, but the horizontal displacement is limited; thus, ux = 0. Additionally, the model's fixed bottom does not allow any displacement; thus, ux = 0, uy = 0, and w = 0.

4.3. Load setting

A double-circular uniform load BZZ-100 was used as the standard axial load in China's highway design requirements, and the parameters are listed in Table 3. Because the equivalent circle diameter of the single wheel pressure transmission surface was 0.213 m, the double circle uniform load may be substituted by the rectangular uniform load, and the tire contact pressure was 0.7 MPa, according to the concept of equivalent area. The rectangular uniform load was 0.213 m × 1 m in size, and the distance between the two rectangular loads was 0.1065 m, or half the corresponding circle diameter. The load was applied to the centre of the road using the area equivalence concept, without considering the impact of different critical load positions on the subgrade. However, BZZ-100 cannot be applied to the model, so BZZ-100 was converted into a two-dimensional linear load according to the static equivalent principle, and its size changed from 0.7 MPa in three-dimension to 117371 N / m in two-dimension, while the size and spacing of the load surface remained unchanged.

For the computational model in this study, the separated model was chosen to embed the BFRP–CRCP into the concrete using the general extrusion function in the COMSOL software, and the slip between the BFRP–CRCP and concrete was not considered; the model was two-dimensional.

In the permafrost locations, BFRP–CRCP was employed to account for the full impact of the melting settlement effect and vehicle load. The single-variable technique was used to investigate the elements affecting the stress of the BFRP–CRCP and the stress characteristics of different pavement combinations to simplify the computation. Figure 2 shows the grid division of the simulation model. Figure 3 shows the pavement stress under specific conditions.

Table 3. BZZ-100 Parameter

Standard axle load	BZZ-100	Standard axle load	BZZ-100
Standard axle load F [kN]	100	Equivalent circle diameter d [cm]	21.30
Tire ground pressure P [MPa]	0.70	Two wheel centre distance [cm]	1.5 d

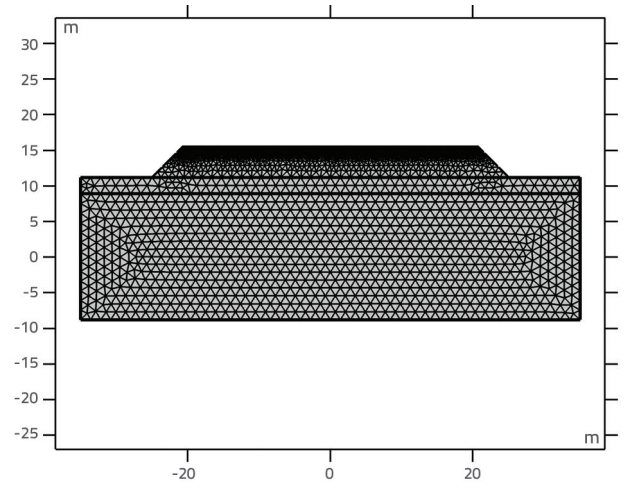

Figure 2. Model meshing

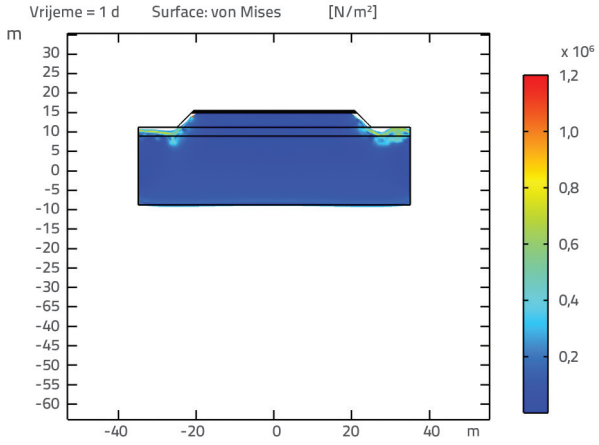

Figure 3. Stress analysis

5. Sensitivity analysis of BFRP–CRCP parameters

Different BFRP–CRCP pavement structure models were created using the single-variable technique and COMSOL software to study the impact of the pavement structure on the BFRP–CRCP stress. Table 4 shows the specific single-factor parameters. The values of the constant pavement parameters are specified in Table 4.

5.1. BFRP–CRCP slab thickness

If the thickness of the BFRP–CRCP pavement slab varies, will it impact the stress of the pavement structure, and what would be the difference between considering and not considering the thaw settling effect? To maintain the other fundamental calculation factors of pavement construction, pavement thicknesses of 20, 22, 24, 26, and 28 cm were selected in this study. Table 5 presents the results, and the maximal principal stress was calculated underneath the slab.

Table 5 shows that considering only the vehicle load (Case1) and considering the thaw settlement and vehicle load coupling (Case 2) have the same change pattern, i.e., when the pavement thickness increases, the maximum primary stress in the pavement decreases consistently. Consequently, increasing the thickness of the BFRP–CRCP panel may effectively minimise the primary stress in the pavement panel.

5.2. BFRP reinforcement ratio

Considering the reinforcement ratios of the BFRP bars as 0.6 %, 0.65 %, 0.7 %, 0.75 %, and 0.8 %, the influence of the

Table 4. Selection of single-factor parameters

Parameters	Setting
BFRP–CRCP slab thickness [cm]	20, 22, 24, 26, 28
Concrete modulus [GPa]	24, 26, 28, 30, 32
Reinforcement ratio [%]	0.60, 0.65, 0.70, 0.75, 0.80
Thickness of base and subbase [cm]	16, 18, 20, 22, 24
Base modulus [GPa]	1.2, 1.3, 1.4, 1.5, 1.6
Subbase modulus [GPa]	1.3, 1.4, 1.5, 1.6, 1.7

Table 5. Maximum principal stress in slabs with different thicknesses

BFRP-CRCP slab thickness [cm]	20	22	24	26	28
Maximum principal stress (without considering thawing settlement) [MPa]	1.210	1.031	0.836	0.724	0.654
Maximum principal stress (considering thawing settlement) [MPa]	2.762	2.581	2.428	2.307	2.206

Table 6. Maximum principal stresses in slabs with different reinforcement ratios

Reinforcement ratio [%]	0.6	0.65	0.7	0.75	0.8
Maximum principal stress (without considering thawing settlement) [MPa]	1.259	1.264	1.270	1.273	1.281
Maximum principal stress (considering thawing settlement) [MPa]	2.635	2.642	2.651	2.658	2.663

Table 7. Maximum principal stress in the slab under different concrete modulus conditions

Concrete modulus [GPa]	24	26	28	30	32
Maximum principal stress (without considering thawing settlement) [MPa]	1.026	1.124	1.218	1.323	1.437
Maximum principal stress (considering thawing settlement) [MPa]	2.564	2.682	2.746	2.867	2.983

Table 8. Maximum principal stress in slabs with different base thicknesses

DBase thickness [cm]	16	18	20	22	24
Maximum principal stress (without considering thawing settlement) [MPa]	1.582	1.476	1.356	1.241	1.125
Maximum principal stress (considering thawing settlement) [MPa]	2.945	2.835	2.702	2.593	2.485

reinforcement ratio on the stress of the pavement structure was studied. The calculation results obtained by keeping the other basic calculation parameters of the pavement structure unchanged are listed in Table 6.

According to Table 6, the reinforcement ratio had a minimal influence on the stress produced by the coupling effect of the vehicle load and settling.

5.3. Elastic modulus of concrete

Maintaining the other fundamental pavement structure calculation parameters constant, the impact of the concrete modulus on the pavement structure stress was investigated using concrete moduli of 24 GPa, 26 GPa, 28 GPa, 30 GPa, and 32 GPa. Table 7 displays the computational results.

As demonstrated in Table 7, the maximum primary stress in the BFRP–CRCP pavement increased with increasing concrete modulus without considering the thawing settling. When the concrete modulus was 24 GPa, the maximum principal stress in the slab was 1.026 MPa; when the concrete modulus was 32 GPa, the maximum principal stress in the slab was 1.437 MPa, an increase of 0.411 MPa; the average modulus of the base increased by 1 GPa and the maximum principal stress of the pavement increased by 0.05 Mpa. When thaw settlement was considered, the maximum principal stress in the BFRP–CRCP pavement slab increased with the increase in concrete modulus. Consequently, the modulus of concrete should be suitably lowered to regulate the internal tension of the pavement slab.

5.4. Base thickness

Keeping the other fundamental pavement structure calculation parameters constant, the thickness of the base was set to 16, 18, 20, 22, and 24 cm to investigate the effect of base thickness on pavement structure stress. Table 8 lists the computational results.

As shown in Table 8, the maximum primary stress in the BFRP–CRCP pavement decreased with increasing base thickness when thawing settling was not considered. When the base layer thickness was 16 cm, the highest primary stress in the slab was 1.582 MPa, and when it was 24 cm, the maximum principal stresses in the slab were 1.125 and 0.457 MPa. The maximum primary stress in the pavement decreased by 0.057 MPa for every 1 cm increase in the base layer thickness. The maximum primary stress in the BFRP–CRCP pavement slab decreased with thaw settling. The highest primary stress in the slab was 2.945 MPa when the base thickness was 16 cm. The highest primary stress in the slab decreased by 0.460 MPa when the base thickness was 24 cm. The maximum primary stress decreased by 0.058 MPa when the base thickness increased by an average of 1 cm. The trend of the maximum primary stress generated in the pavement slab changing with the thickness of the base is the same, whether merely considering the vehicle load or including the coupled impact of thaw settling and the vehicle. Consequently, while constructing continuous reinforced concrete pavements in permafrost locations, the base thickness should be adequately increased to regulate the stress conditions in the pavement slab.

Table 9. Maximum principal stress in the slab under different base moduli

Base modulus [GPa]	1.2	1.3	1.4	1.5	1.6
Maximum principal stress (without considering thawing settlement) [MPa]	1.426	1.323	1.271	1.168	1.105
Maximum principal stress (considering thawing settlement) [MPa]	2.654	2.758	2.849	2.986	3.142

Table 10. Maximum principal stress in the slab under different subbase thicknesses

Subbase thickness [cm]	16	18	20	22	24
Maximum principal stress (without considering thawing settlement) [MPa]	1.442	1.375	1.308	1.243	1.154
Maximum principal stress (considering thawing settlement) [MPa]	2.993	2.924	2.862	2.802	2.728

5.5. Base modulus

The impact of the base thickness on the pavement structure stress was investigated using the base moduli of 1.2, 1.3, 1.4, 1.5, and 1.6 GPa, keeping the other fundamental pavement structure calculation parameters constant. Table 9 lists the computational results.

Without considering the thaw settlement, the maximum primary stress in the BFRP–CRCP pavement decreased as the base modulus increased, as shown in Table 9. The greatest primary stress in the slab was 1.426 MPa when the base modulus was 1.3 GPa. The highest primary stress in the slab was 1.105 MPa when the base modulus was 1.6 GPa, a decrease of 0.321 MPa. The maximum primary stress of the pavement decreased by 0.064 MPa when the base modulus increased by 100 MPa. In terms of the thaw settlement, the maximum primary stress in the BFRP–CRCP pavement slab increased as the base modulus increased. When the base modulus was 1.3 GPa, the highest principal stress in the slab was 2.654 MPa. When the base modulus was 1.6 GPa, the maximum principal stress in the slab was 3.142 MPa, an increase of 0.488 MPa, and for every 100 MPa increase in the base modulus, the maximum principal stress increased by 0.098 MPa. The change trend of the maximum primary stress of the pavement slab differed based on the increasing base modulus, solely considering the vehicle load, and considering the coupling of thawing settlement and vehicle load. Therefore, to decrease the stress in the pavement slab, a low-modulus foundation should be used to BFRP–CRCP pavements in frozen soil areas.

5.6. Subbase thickness

Keeping the other fundamental pavement structure calculation parameters constant, the thicknesses of the base layer were 16, 18, 20, 22, and 24 cm to investigate the effect of base layer thickness on pavement structure stress. Table 10 lists the computational results.

Without considering the thawing settlement, the maximum primary stress in the BFRP–CRCP pavement decreased as the subbase thickness increased, as listed in Table 10. The highest primary stress in the pavement was 1.442 MPa when the subbase thickness was 16 cm. The highest primary stress in the pavement was 1.154 MPa when the subbase thickness was 24 cm, a decrease of 0.288 MPa. The maximum primary stress in the pavement decreased by 0.036 MPa on average as the thickness of the subbase increased by 1 cm. When the thaw settlement effect was considered, the maximum primary stress in the BFRP–CRCP pavement decreased as the subbase thickness increased; the maximum primary stress was 2.993 MPa when the subbase thickness was 16 cm. When the subbase thickness increased to 24 cm, the maximum primary stress was 2.728 MPa, a decrease of 0.265 MPa. When the thickness of the subbase increased by an average of 1 cm, the maximum primary stress decreased by 0.033 MPa. Whether merely considering the vehicle load or including the coupling impact of the thaw settlement and vehicle, the fluctuation trend of the maximum primary stress in the pavement with the base-layer thickness was the same. As a result, in permafrost zones, correctly increasing the thickness of the base layer is also effective in controlling the stress conditions in the pavement.

5.7. Subbase modulus

Keeping the other fundamental calculation parameters of the pavement structure constant, the impact of the base modulus on the stress of the pavement structure was investigated using the base moduli of 1.3, 1.4, 1.5, 1.6, and 1.7 GPa. Table 11 shows the computational results.

Without considering the thawing settlement, the maximum primary stress in the BFRP–CRCP pavement decreased as the subbase modulus increased, as shown in Table 11. The highest primary stress in the slab was 1.356 MPa when

Table 11. Maximum principal stress in the slab under different subbase moduli

Subbase modulus [GPa]	1.3	1.4	1.5	1.6	1.7
Maximum principal stress (without considering thawing settlement) [MPa]	1.356	1.304	1.243	1.208	1.169
Maximum principal stress (considering thawing settlement) [MPa]	2.785	2.832	2.894	2.966	3.065

Table 12. Pavement structure combinations

Structure combination 1	**Structure combination 2**	**Structure combination 3**
BFRP–CRCP road panel	BFRP–CRCP road panel	BFRP–CRCP road panel
Cement stabilized macadam	Graded crushed stone	ATB-25
Lime soil	Cement stabilized macadam	Cement stabilized macadam

Table 13. Material specifications of each structural layer

Material parameters	**BFRP–CRCP road panel**	**Graded crushed stone**	**Lime soil**	**Cement stabilized macadam**	**ATB-25**
Layer thickness [cm]	20 – 28	16 – 24	20	20	12
Modulus [GPa]	2.4–3.2	0.3	1.5	1.2	1.2

the base modulus was 1.3 GPa. The highest primary stress in the slab was 1.169 MPa when the base modulus was 1.7 GPa, a decrease of 0.187 MPa. The maximum primary stress of the pavement decreased by 0.037 MPa when the base modulus increased by 100 MPa. When thaw settlement occurred, the maximum primary stress in the pavement of base modulus increased as the base modulus increased. The highest primary stress in the slab was 2.785 MPa when the base modulus was 1.3 GPa. When the base modulus was 1.7 GPa, the maximum primary stress in the slab increased by 0.28 MPa to 3.065 MPa. The maximum primary stress in the pavement increased by 0.056 MPa when the base modulus increased by an average of 100 MPa. Under the two different conditions of considering and not considering the thawing settlement, the impact of the subbase modulus on the maximum primary stress in the pavement was entirely opposite. According to the coupling effect, as the modulus increased, the maximum primary stress also increased. Consequently, to decrease pavement stress, the modulus of the subbase should be adequately lowered.

5.8. Combined stress characteristics of different BFRP–CRCP pavement structures

Table 12 shows the three most widely utilised structural combinations of CRCP based on the structural properties of the BFRP–CRCP pavement and the thawing settlement impact of frozen soil in Northeast China. The optimal combination was selected after comparing the effects of the layer thickness and modulus on the pavement structure. Table 13 lists the material specifications of each structural layer.

1. Influence of the pavement slab thickness

Figure 4 depicts the maximum stress change in the slab for three distinct pavement combinations with various slab thicknesses.

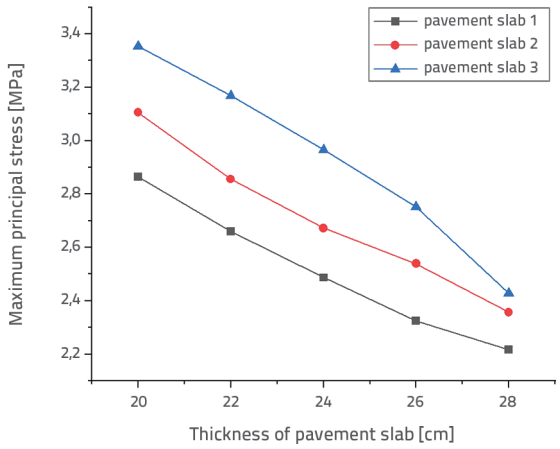

Figure 4. Variation trend of maximum principal stress under different thicknesses and structures of the pavement slab

As demonstrated in Figure 4, the maximum primary stress in structures 1, 2, and 3 steadily reduced as the thickness of the pavement slab increased. When the pavement thickness was 20 cm, the maximum primary stress of the structures 1, 2, and 3 were 2.865, 3.106, and 3.353 MPa, respectively. When the pavement thickness was 28 cm, the corresponding maximum primary stresses were 2.216, 2.357, and 2.428 MPa, corresponding to decreases of 0.649, 0.749, and 0.925 MPa, respectively. The maximum primary stress in structure 3, with

the asphalt macadam layer, was the highest and was most affected by the slab thickness.

2. Effect of concrete modulus

Figure 5 shows the maximum stress change in the slab for three distinct pavement combinations with varying concrete elastic moduli.

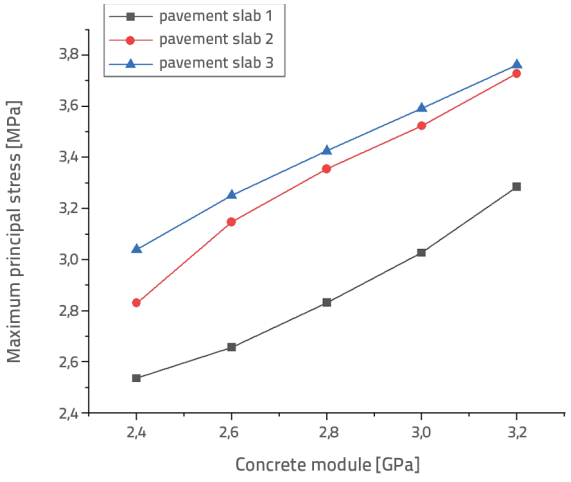

Figure 5. Variation trend of maximum principal stress in composite slabs with different concrete moduli and structures

As shown in Figure 5, as the concrete modulus increased, the maximum primary stress in the slabs of structures 1, 2, and 3 increased. When the concrete modulus was 2.4 GPa, the maximum primary stress of structures 1–3 was 2.536, 2.831, and 3.039 MPa, respectively. When the concrete modulus was 3.2 GPa, the maximum primary stresses were 3.285, 3.728, and 3.762 MPa, corresponding to increases of 0.749, 0.897, and 0.723, respectively. It can be observed that concrete modulus has a significant impact on structures 1 and 3.

3) Influence of graded gravel thickness

Figure 6 shows the maximum stress change in the slab for three distinct pavement combinations with varying graded gravel thicknesses.

As shown in Figure 6, the maximum primary stress in the slabs of Structures 1, 2, and 3 decreased as the thickness of the graded gravel increased. The maximum primary stresses of structure 1, 2, and 3 were 3.128, 3.248, and 3.475 MPa, respectively, when the graded gravel thickness was 16 cm. When the graded gravel thickness was 24 cm, the maximum primary stresses were 2.628, 2.786, and 2.832 MPa, corresponding to decreased of 0.50, 0.462, and 0.643 MPa, respectively.

Based on the magnitude of the maximum primary stress in cement concrete pavements, there are three types of pavement structure combinations: structure 1 < structure 2 < structure 3.

On examining the impact of the thawing settlement, it is clear that structure 1 is the best BFRP–CRCP pavement structure for permafrost environments.

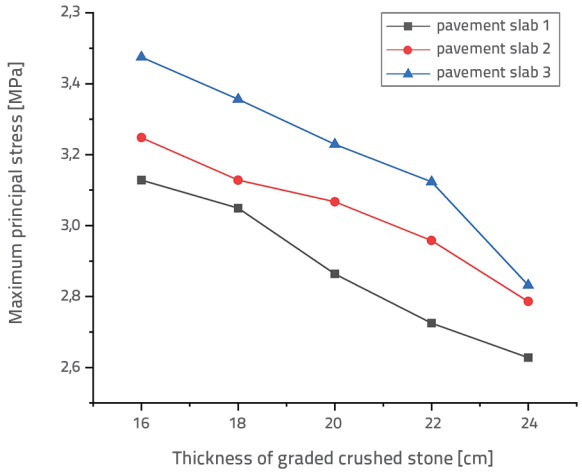

Figure 6. Variation trend of maximum principal stress under different graded gravel thicknesses and structure combination of the slab

6. Conclusion

Continuous reinforced concrete pavements with basalt fibre reinforcement are being built in the permafrost zones of Northeast China. The stress characteristics of the BFRP–CRCP pavement in permafrost locations were analysed using the COMSOL finite element software, providing a foundation for the development of appropriate BFRP–CRCP pavement structures in Northeast China. The key conclusions are as follows.

- The influence of the thaw settlement effect on the stress characteristics of the pavement structure was significant in the building of BFRP–CRCP pavements in Northeast China. The vehicle load alone cannot be regarded in the design, and the effects of thaw settling effect must be properly recognized as well, because the maximum primary stress created by the coupling effect of thaw settlement impact and vehicle load on pavement increases with time in permafrost zones.
- Regarding the stress characteristics under the coupling effect, increasing the thicknesses of the slab, base, and subbase reduced the maximum primary stress of the pavement. Simultaneously, increasing the moduli of the concrete, base, and sub-base increased the maximum primary stress of the pavement. The stress state was unaffected by the reinforcement ratio.
- Of the three pavement structure combination forms, the pavement structure of BFRP–CRCP pavement + water-stabilised gravel foundation + lime soil base was more suitable for the northeast permafrost zone, if only in terms of decreasing the maximum primary stress of the pavement.

REFERENCES

[1] Gáspár, L., Bencze, Z.: Increasing the life expectancy of road pavements, GRADEVINAR, 72 (2020) 6, pp. 515-522, https://doi.org/10.14256/JCE.2644.2019.

[2] Stijanović, M., Radonjanin, V., Malešev, M., Milović, T., Furgan, S.: Compressive strength of cement stabilisations containing recycled and waste materials, GRADEVINAR, 73 (2021) 8, pp. 791-804, https://doi.org/10.14256/JCE.3161.2021.

[3] Dongwei, C., Changshun, H.: Temperature relaxation stress analysis of CRCP concrete, China Journal of Highways, 14 (2001) 1, pp. 1-4.

[4] Garnham, M.A.: The development of CRCP design curves", Highways & Transportation, 36 (1998) 12, pp. 259-281.

[5] Minghui, Z., Unk, U.: Structural analysis and engineering application of continuous reinforced concrete pavement, Doctoral dissertation, Nanhua University, 2015.

[6] Wang, X.: Research on basic theory test and design method of continuous reinforced concrete pavement, Doctoral dissertation, Southeast University,1990.

[7] Yimin, T., Xiaoming, H., Xuejun, D.: Load stress analysis of continuous reinforced concrete pavement, Geotechnical Engineering Journal, 18 (1996) 6, pp. 88-95.

[8] Gao, Y., Huang, X., Chen, C.: Design method of reinforcement ratio of continuous reinforced concrete pavement based on reliability, Journal of Southeast University (Natural Science Edition), 39 82009) 4, pp. 835-839.

[9] Zhou, Y.: Temperature stress analysis and reinforcement design of continuous reinforced concrete pavement in cold regions, Doctoral dissertation, 2006.

[10] Zuo, Z., Zhang, H., Wang, Y.: Field test and analysis of early mechanical response of continuous reinforced concrete pavement, Chinese Journal of Highway, 23 (2010) 3, pp. 22-28.

[11] Gu, X., Lu, J., Wang, W.: Analysis and comparison of basalt fibre reinforcement and reinforcement in pavement application, Highway, 12 (2009), pp. 54-57.

[12] Ming, E.: Structural mechanics analysis of basalt fibre reinforced continuous reinforced concrete pavement considering impact failure, Doctoral dissertation, South China University of Technology, 2015.

[13] Xu, Z.: Mechanical analysis and design method of continuous reinforced concrete pavement with BFRP bars, Doctoral dissertation, South China University of Technology, 2017.

[14] Fang, F.: Experimental study on the bonding performance of basalt fibre reinforced concrete, Doctoral dissertation, Dalian University of Technology, 2009.

[15] Zhang, X.: The bond-slip characteristics and construction technology of BFRP continuous reinforcement composite pavement materials, Doctoral dissertation, Zhejiang University, 2014.

[16] Ji, J., Gu, X., Lu, J., et al.: Research on Construction Technology of Continuous Basalt Fiber Reinforced Cement Concrete Pavement, Highway Traffic Technology (Applied Technology Edition), 5 (2009) 5, pp.37-39.

[17] Yu, L., Qiu, J., Wang, Z.: Study on the frost heaving coupling model of roads in Changchun City, Journal of Harbin Institute of Technology, 4 (2011), pp. 291-294.

[18] Mao, X., Li, N., Wang, B., et al.: Water-thermal-mechanical coupling theoretical model and numerical simulation of permafrost subgrade, Natural Science Edition, 26 (2006) 4, pp. 16-19.

[19] Li, N., Xu, B., Chen, F.: The coupling analysis of temperature field, deformation field and stress field of frozen soil subgrade, Chinese Journal of Highway, 19 (2006) 3, pp. 1-7.

[20] Zhu, Z., Ning, J., Ma, W.: Research on constitutive model of frozen soil based on damage and numerical simulation of water, heat and force coupling, Scientific Report, 21 (2010), pp. 758-772.

[21] Zhou, J., Tan, T., Wei, C.: Experimental study on freezing temperature and supercooling temperature of soil, Geotechnical mechanics, 36 (2015) 3.

[22] Li, S., Lai, Y., Pei, W., et al.: Moisture–temperature changes and freeze–thaw hazards on a canal in seasonally frozen regions, Natural Hazards, 72 (2014) 2, pp. 287-308.

[23] Wang, W., Wang, L., Wang, Q.: Study on one-dimensional melting and consolidation characteristics under periodic temperature boundary conditions, Glacier Permafrost, 36 (2014) 4, pp. 895-901.

[24] Ottosen, N.S.: A failure criterion for concrete", Journal of Engineering Mechanics Division, ASCE, 103 (1977), pp. 527-535.

[25] Hu, Z.: The characteristics of permafrost degradation in the north of Xiaoxing' an Mountains and its influence on the stability of highway subgrade, Doctoral dissertation, Northeast Forestry University, 2017.

[26] Lai, Y., Zhang, L., Zhang, S.: Cooling effect of rubble subgrade on Qinghai–Tibet Railway under climate warming, Scientific Bulletin, 3 (2003), pp. 292-297.

[27] Yin, D.: Study on continuous reinforced concrete pavement in permafrost regions Doctoral dissertation, Southeast University, 2019.

[28] Mingli, Z., Zongyun, G., Xiaobin, H., et al.: Analysis of coupled water and heat transfer in frozen soil based on mathematical module of COMSOL multiphysics, Science Technology and Engineering, 18 (2018) 33, pp. 7-12.

[29] Jianbing, C.: Theoretical model of three-field coupling analysis of highway subgrades in permafrost regions under freeze–thaw cycles, Highway, 60 (2015) 10, pp. 7.

[30] Linnan, Z.: Study on the Interfacial Layers of Different Underlying Surfaces in Plateau Permafrost Regions, Journal of Glaciology and Geocryology, 10 (1988) 1, pp. 8-14.